Journal of Civil Engineering and Management
ISSN 1392-3730 / eISSN 1822-3605
2022 Volume 28 Issue 3: 223–231
https://doi.org/10.3846/jcem.2022.16609

A NEW CONSTITUTIVE MODEL FOR THE TIME-DEPENDENT BEHAVIOR OF ROCKS WITH CONSIDERATION OF DAMAGE PARAMETER

Sara EBRAHIMI ZOHRAVI[1], Ali LAKIROUHANI[1], Hamed MOLLADAVOODI[2], Jurgis MEDZVIECKAS[3*], Romualdas KLIUKAS[4]

[1]*Department of Civil Engineering, Faculty of Engineering, University of Zanjan, Zanjan, Iran*
[2]*Department of Mining and Metallurgical Engineering, Amirkabir University of Technology, Tehran, Iran*
[3]*Department of Reinforced Concrete Structures and Geotechnics, Vilnius Gediminas Technical University, Saulėtekio al. 11, 10223 Vilnius, Lithuania*
[4]*Department of Applied Mechanics, Vilnius Gediminas Technical University, Saulėtekio al. 11, 10223 Vilnius, Lithuania*

Received 18 November 2021; accepted 25 February 2022

Abstract. Deformation and time-dependent behavior of rocks are closely related to the stability and safety of underground structures and mines. In this paper, a numerical-analytical model is presented to investigate time-dependent damage and deformation of rocks under creep. The proposed model is obtained by combining the elastic-visco-plastic model based on the theory of over-stress and stress hardening law with the sub-critical crack growth model. The advantage of this model is that it is in incremental form and therefore can be implemented numerically. First, the governing equations of the model and its numerical computational algorithm are described. The proposed constitutive model is then implemented in the FLAC code using the FISH function. Determination of model parameters and calibration is done by various laboratory tests performed on a type of gypsum. The creep test was performed on gypsum under a stress of 13 MPa, which is equal to 70% of its compressive strength. After determining the parameters, by fitting the creep curve of the presented analytical-numerical model, a good agreement is observed with the creep curve obtained from the laboratory data. It is also observed that during creep, the damage parameter and wing crack length increase.

Keywords: elastic-visco-plastic model, over-stress theory, sub-critical crack growth, creep test, stress hardening, wing crack.

Introduction

The study of time-dependent behaviour of rocks, commonly known as creep, is of particular importance in rock mechanics and the design of underground structures, because the time-dependent behavior of rocks is closely related to the stability and safety of underground structures and tunnels. Rock specimens subject to a constant stress, creep conditions, deform at a variable strain rate over time. The strain-versus-time curve usually has three steps in the creep test: primary creep, secondary creep, and tertiary creep, provided the stress on the sample is high enough. Various constitutive models have been proposed to investigate the time-dependent behavior of soils and rocks. The proposed models are divided into three categories: empirical models, rheological models, and general stress-strain theories. Empirical models are based on the results of laboratory data and field experiments (Lomnitz, 1956; Griggs & Coles, 1954; Aydan et al., 2014; Robertson, 1955; Afrouz & Harvey, 1974). Rheological models are obtained by combining simple models such as the Hook model (spring), Saint-Venant's model (slider), and the Newtonian model (viscous dashpot) in series or in parallel (Goodman, 1989). Rheological models have the ability to predict the visco-elastic or elastic-visco-plastic behavior of materials (Gioda & Civdini; 1996; Sterpi & Gioda, 2009). Simple visco-elastic models include the Maxwell model, Kelvin model, Burger model, the generalized Maxwell model, the generalized Kelvin model, and the Zener model (Aydan, 2016). General stress-strain

*Corresponding author. E-mail: *jurgis.medzvieckas@vilniustech.lt*

models are often incremental and are commonly used in analysis based on numerical methods, and are therefore recommended in engineering applications.

Perzyna's over-stress theory is a general theory for the elastic-visco-plastic behavior model of materials, which predicts not only time-dependent behavior but also time-independent behavior of the materials (Perzyna, 1966). This model, which is based on the concept of moving yield surface is applicable to all boundary conditions and all stress paths. In moving yield surface theory, the yield function is directly dependent on time and is continuously changing. The most important models based on Perzyna's over-stress theory are Lemaitre's (Lemaitre & Chaboche, 1990) and SHELVIP (Debernardi & Barla, 2009) models. One of the advantages of the SHELVIP (Debernardi & Barla, 2009) model is that the hardening function depends on the stress level. In almost all models, hardening is controlled using a scalar value such as visco-plastic deviatoric strain, the exact amount of which cannot be determined in the laboratory (Debernardi & Barla, 2009).

But, based on laboratory studies, it has been observed that creep in the rock is associated with the damage (Shao et al., 2006; Ma et al., 2017). Damage models are classified into phenomenological and micro-mechanical models. In phenomenological models, the damage variable is determined using the mechanical properties of the rock at the macro-scale (Hou et al., 2019). Phenomenological models include Lemaitre's model (Lemaitre & Chaboche, 1990) and Pellet's model (Pellet et al., 2005), which are based on the definition of surface damage variable. It is also possible to evaluate the behavior of the rock by combining phenomenological damage models and visco-plastic models (Hou et al., 2019; Zhang et al., 2019; Huang et al., 2020; Feng et al., 2020).

In micro-mechanical models, the effect of microstructure on rock behavior is considered. One of the micro-mechanical damage models, which is highly consistent with the creep behavior of rock, is the sub-critical crack growth model (Lockner, 1993; Lockner & Madden, 1991; Kemeny, 1991). This model is well adapted to the creep of rock materials because according to this theory, the growth of micro-cracks is a time-dependent phenomena and its onset occurs at a stress intensity factor less than the fracture toughness of the rock (Ko & Kemeny, 2013).

The purpose of this paper is to integrate the stress hardening elastic-visco-plastic constitutive model with the sub-critical crack growth damage criterion. The elastic-visco-plastic model is based on the general theory of over-stress. By adding the sub-critical crack growth damage model to it, it becomes a comprehensive model that simulates the creep behavior of the rock in the primary and secondary stages. In most practical cases, the stress level is rarely so high that the rock enters the tertiary stage of creep. In other words, before the rock enters the tertiary stage of creep, the displacements increase so much that the structure falls in terms of profitability.

Thus, first, in Section 1, the equations governing the elastic-visco-plastic model with stress hardening are given, then the sub-critical crack growth model is explained. In the Section 2, the numerical solution algorithm is presented in the form of a flowchart. Section 3 deals with the determination of model parameters and calibration. Calibration is done using various tests performed on a type of gypsum. In the Section 4, a comparison is made between the creep curve obtained from the analytical-numerical model and the creep curve obtained from the creep test of gypsum rock samples.

1. Elastic-visco-plastic constitutive model

The rock medium is assumed to be dry, continuous, homogeneous and isotropic. The model presented in this article is a combination of elastic model, plastic model and visco-plastic model base on over-stress theory of Perzyna (1966). According to the over-stress theory, during loading, a stress state can exceed the yield surface, which is contrary to the classical elasto-plastic theory. Figure 1 shows the general form of yield surfaces and the stress spaces between them in the principal stress space. In this model, two yield surfaces with time-dependent behavior are considered: visco-plastic yield surface and the perfect plastic yield surface. Yield surfaces based on the Drucker-Prager failure criterion divide the stress space into three stress fields as shown in Figure 1. It is assumed that the plastic yield surface is always fixed and does not harden during increasing plastic strain and visco-plastic strain, but the visco-plastic yield surface hardens. The stress fields between the yield surfaces are described below.

1) Elastic stress field: inside the visco-plastic yield surface, the deformations follow an elastic constitutive model. The elastic stress field is important for modeling under small stress conditions as well as unloading. In this field the strain is simply obtained based on the equation governing the theory of elasticity:

$$\varepsilon_{ij} = \varepsilon_{ij}^{e}, \tag{1}$$

where ε_{ij}^{e} is the elastic strain.

2) Visco-plastic stress field: it is located between the visco-plastic yield surface and the plastic yield surface. This stress field also includes its previous stress field, which is omitted due to its brevity. In this space, the total strain is the sum of the elastic strain and the visco-plastic strain (Hasanzadehshooiili et al., 2012):

$$\varepsilon_{ij} = \varepsilon_{ij}^{e} + \varepsilon_{ij}^{vp}, \tag{2}$$

where visco-plastic strain ε_{ij}^{vp} is calculated using the visco-plastic flow rule.

3) Plastic stress field: this field is located on the plastic yield surface, every point in this stress field has a stress path that has passed through the previous fields, which due to brevity their names are omitted. Therefore, the total strain in the plastic stress field is given by:

$$\varepsilon_{ij} = \varepsilon_{ij}^{e} + \varepsilon_{ij}^{vp} + \varepsilon_{ij}^{p}, \tag{3}$$

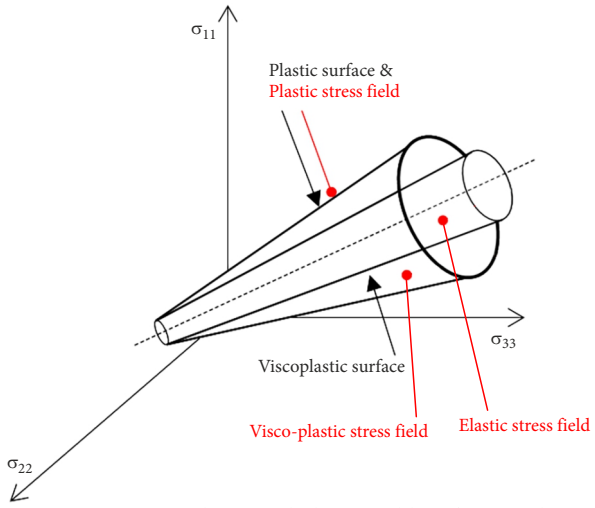

Figure 1. Visco-plastic and plastic yield surfaces in the principal stress space (Debernardi & Barla, 2009)

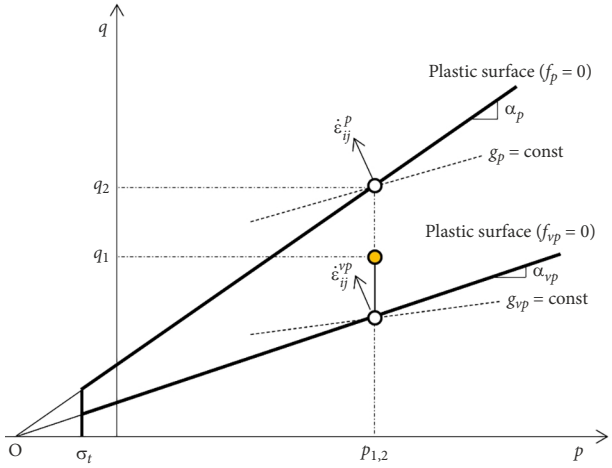

Figure 2. Yield surfaces and the spaces between them in the q-p coordinates (Debernardi & Barla, 2009)

where plastic strain ε_{ij}^{p} is calculated using the plastic flow rule. Figure 2 shows these yield surfaces and the spaces between them in the *q-p* coordinates, where

$$p=\frac{1}{3}(\sigma_{ii}),\ q=\sqrt{\frac{3}{2}S_{ij}S_{ij}}; \tag{4}$$

$\sigma_{ii},(i=1-3)$ are the principal stresses, and $S_{ij},(i,j=1-3)$ are the components of the deviatoric stress tensor.

1.1. Yield surfaces definition

The yield surfaces are based on the Drucker-Prager linear failure criterion, the equation of plastic yield surface (f_p) in the *q-p* plane is as follows (Lakirouhani & Hasanzad-ehshooiili, 2011):

$$f_p=q-\alpha_p.p-k_p \text{ for } p\geq\sigma_t, \tag{5}$$

where α_p, k_p as shown in Figure 2, are the slope and q-intercept of the Drucker-Prager linear failure criterion.

The relationship between the Drucker-Prager parameters and the Mohr-Coulomb parameters in the circumscribed Drucker–Prager failure criterion and the inscribed Drucker–Prager failure criterion are as follows, respectively:

$$\alpha_p=\frac{6}{3-\sin\phi}\sin\phi,\quad k_p=\frac{6c}{3-\sin\phi}\cos\phi; \tag{6}$$

$$\alpha_p=\frac{6}{3+\sin\phi}\sin\phi,\quad k_p=\frac{6c}{3+\sin\phi}\cos\phi, \tag{7}$$

where c,ϕ are cohesion and internal friction angle of the rock material. The visco-plastic yield surface (f_{vp}) is defined as Eqn (8), assuming that this yield surface intersects the plastic yield surface at point O, as shown in Figure 2:

$$f_{vp}=q-\alpha_{vp}(p+\frac{k_p}{\alpha_p}) \text{ for } p\geq\sigma_t, \tag{8}$$

α_{vp} is the slope of visco-plastic yield surface in the q-p plane. In Figure 2, σ_t represents the tensile strength of the rock.

1.2. Calculation of strain rates

The elastic strain rate component $\dot{\varepsilon}_{ij}^{e}$ is obtained using the Hooke's law:

$$\dot{\varepsilon}_{ij}^{e}=C_{ijkl}\,\dot{\sigma}_{kl}, \tag{9}$$

where $\dot{\sigma}_{kl}$ is the stress rate tensor and C_{ijkl} is a fourth-order elasticity tensor (material elasticity tensor) whose components depends on Young's modulus E and Poisson's ratio υ as follows:

$$C_{ijkl}=\frac{1}{E}\left[(1+\upsilon)\delta_{ik}\delta_{jl}-\upsilon\,\delta_{ij}\delta_{kl}\right], \tag{10}$$

where δ_{ij} is the Kronecker delta defined by:

$$\delta_{ij}=\begin{cases}1 & \text{if } i=j\\ 0 & \text{if } i\neq j\end{cases}. \tag{11}$$

To calculate the visco-plastic strain rate $\dot{\varepsilon}_{ij}^{ve}$, the flow rule is derived from the Perzyna's over-stress theory (Perzyna, 1966), as follows:

$$\dot{\varepsilon}_{ij}^{vp}=\gamma\,\Phi(F)\frac{\partial g_{vp}}{\partial\sigma_{ij}}, \tag{12}$$

where γ is fluidity parameter which controls the amplitude of visco-plastic strain rate, $\Phi(F)$ is the viscous kernel and F is the over-stress function. In the model presented in this paper, it is assumed that the over-stress function is equal to the visco-plastic yield function presented in Eqn (8), i.e., $F=f_{vp}$. Also g_{vp} is visco-plastic potential function. The visco-plastic kernel $\Phi(F)$ determines the magnitude of the visco-plastic strain rate and is considered as a power function of the over-stress function F as follows:

$$\Phi(F)=\{F\}^n=\begin{cases}0 & \text{if } F<0\\ F^n & \text{if } F>0\end{cases}, \tag{13}$$

where $n>0$ is a characteristic parameter, and $\{\ \}$ is the Macaulay brackets. The visco-plastic potential function g_{vp} expresses the direction of the visco-plastic strain rate tensor, which is defined as:

$$g_{vp} = q - \omega_{vp} p. \tag{14}$$

In other words, g_{vp} it is a linear function of deviatoric stresses and volumetric stresses. ω_{vp} is the visco-plastic dilatancy, which is equal to the ratio of the volumetric visco-plastic strain changes to the deviatoric visco-plastic strain increment. By substituting Eqn (13) and Eqn (14) in relation (12) and assuming that $F = f_{vp}$, relation (12) becomes as:

$$\dot{\varepsilon}_{ij}^{vp} = \gamma \left\{ f_{vp} \right\}^n \left(\frac{3}{2} \frac{S_{ij}}{q} - \frac{1}{3} \omega_{vp} \delta_{ij} \right), \tag{15}$$

where S_{ij} are the components of the deviatoric stress tensor and δ_{ij} is the Kronecker delta according to Eqn (11). Finally, the plastic strain rate is calculated using the elasto-plastic flow rule as:

$$\dot{\varepsilon}_{ij}^{p} = \lambda \frac{\partial g_p}{\partial \sigma_{ij}}, \tag{16}$$

where λ is the plastic coefficient, and g_p is the plastic potential function, which is defined as follows, assuming non-associated flow rule:

$$g_p = q - \omega_p p, \tag{17}$$

where ω_p is the plastic dilatancy, which is equal to the ratio of the volumetric plastic strain changes to the deviatoric plastic strain increment.

1.3. Hardening rule for visco-plastic yield surface

In the SHELVIP model, Debernardi and Barla (2009) proposed a stress-based hardening rule in which the time derivative of α_{vp} relates to the stress state $f_{vp}\left(\sigma_{ij}\right)$ as:

$$\dot{\alpha}_{vp} = \frac{\ell}{mn} \frac{f_{vp}}{p + \frac{k_p}{\alpha_p}} \left(\frac{f_{vp}}{q} \right)^{mn}, \tag{18}$$

where m is the shape factor that define the shape of creep curves and ℓ is the time stretching factor, both are characteristic and positive parameters.

1.4. Sub-critical crack growth

In the model developed in this paper, the pre-critical damage model is used to predict rock damage in creep. In this mechanism, before the stress intensity factor reaches its critical value, i.e., fracture toughness, the cracks in the sample start to grow and develop as the stress intensity factor increases (Lockner & Madden, 1991). Sub-critical crack growth can occur under static or dynamic loading conditions. For example, under static loading, crack growth velocity is a power law function of the stress intensity factor (Lockner & Madden, 1991; Ko et al., 2006). Figure 3 shows the crack velocity versus the normalized stress intensity factor, for sub-critical crack growth. In region 1, the crack velocity is sensitive to stress (Lockner, 1993). The stress intensity factor in region 1 is approximately between $0.2K_c$ and $0.8K_c$ (Ko & Kemeny, 2013), where K_c is fracture toughness. If the crack is subjected to

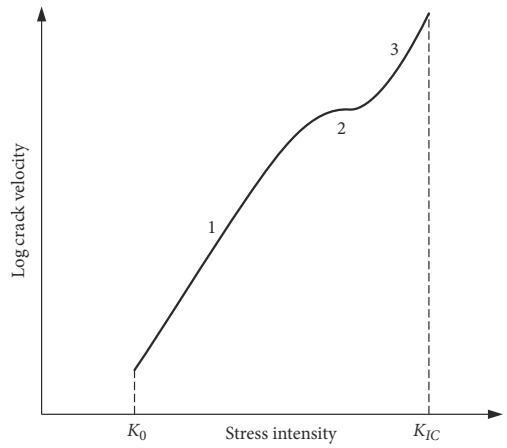

Figure 3. Experimental typical relationship between crack velocity and normalized stress intensity factor (Lockner & Madden, 1991)

stress intensity factor less than $0.2K_c$, then it will not be able to develop. This model is suitable for simulating rocks in creep experiments, since the time-dependent strain in creep tests are mainly due to the micro-cracks growth (Kranz, 1979, 1980).

According to the theory of sub-critical crack growth, the crack growth function is presented as:

$$f_d = \frac{K_I}{K_{Ic}} - 0.2, \tag{19}$$

as long as $f_d > 0$, cracks growth. In Eqn (19), K_I is the stress intensity factor in mode I and K_{Ic} is the fracture toughness corresponding to this mode.

A power law function is then used for the crack velocity v (Lockner & Madden, 1991; Olson, 1993; Ko et al., 2006; Ko & Kemeny, 2013):

$$\nu = \dot{a} = A \left(\frac{K_I}{K_{Ic}} \right)^r, \tag{20}$$

where $\dot{a}$ is the crack growth rate, and A and r are the sub-critical crack growth parameter and the sub-critical crack growth index, respectively.

1.5. Micro-mechanical damage model and stress intensity factor

We used the micro-mechanical damage model to calculate the stress intensity factor. In this method, a dilute uniformly distribution of pre-existing flaws (closed cracks) within the material is assumed which have no interaction on each other. Due to the application of compression loading on the sample, there is a tendency for frictional slip on the flaw surfaces, which causes wing cracks to grow in the flaw tips (Figure 4). It has been proved that the nucleation of wing cracks occurs at $\theta = 70.5°$ (Paliwal & Ramesh, 2008; Ashby & Hallam, 1986; Horii & Nemat-Nasser, 1986). The principle of superposition is used to calculate the stress intensity factor at the tip of the wing cracks. To calculate the first term of the stress intensity factor, two wing cracks of length a are replaced by a straight crack of

length 2*a*, which is affected by the same external stresses. The second term of the stress intensity factor is caused by stresses induced by the flaw under the same external loads. Finally, the stress intensity factor is given by Horii and Nemat-Nasser (1986):

$$K_I = -\frac{2\,s\,\tau_{eff}\sin\theta}{\sqrt{\pi(a+0.27s)}} + \frac{1}{2}\sqrt{\pi a}\Big[(\sigma_1+\sigma_3)+ (\sigma_1-\sigma_3)\cos 2(\theta+\beta)\Big]. \quad (21)$$

In this equation, s is half the flaw length (Figure 4), and τ_{eff} is the effective shear stress on the flaw surface, which is obtained as:

$$\tau_{eff} = \frac{1}{2}(\sigma_1-\sigma_3)\sin 2\beta - \mu\left[\frac{1}{2}(\sigma_1+\sigma_3)+ (\sigma_1-\sigma_3)\cos 2\beta\right] - \tau_c, \quad (22)$$

where μ and τ_c are the coefficient of friction and cohesion on the flaw surface, respectively, it is often assumed $\tau_c = 0$.

1.6. Damage parameter

Evolution of damage occurs during increasing wing crack length, to evaluate it, it is necessary to define the damage parameter, so that its changes can be examined in proportion to the increase in the strain and creep progression. The damage parameter is defined from a phenomenological point of view as the ratio of micro-cracks area to total area, but in this paper, it is discussed based on micro-mechanics. The damage parameter (Ω) in two-dimensional condition, is given by Paliwal and Ramesh (2008):

$$\Omega = \eta\, a^2, \quad (23)$$

where η is the flaw density i.e., the number of flaw per unit area (in unit of $1/m^2$), and a is the wing crack length, which is related to the stress intensity factor by Eqn (21). Therefore, the evolution of the damage parameter with time is equal to

$$\dot{\Omega} = 2\eta a\dot{a}. \quad (24)$$

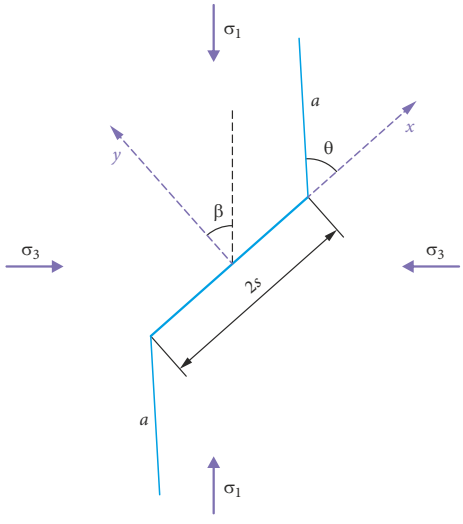

Figure 4. A flaw with the wing cracks at its tips

1.7. Homogenization

What remains of the micro-mechanical damage model is homogenization. Using the damage parameter defined in the previous section, and assuming a dilute (non-interacting) flaw distribution, the effective elastic constants are defined as (Gross & Seelig, 2018):

$$K^{\hom} = K\left[1 - \frac{16}{9}\frac{(1-\upsilon^2)}{(1-2\upsilon)}\Omega\right]; \quad (25)$$

$$G^{\hom} = G\left[1 - \frac{32}{45}\frac{(1-\upsilon)(5-\upsilon)}{(2-\upsilon)}\Omega\right]. \quad (26)$$

2. Numerical implementation and algorithm

The computational algorithm of the mathematical model presented in Section 1 is shown in Figure 5. Using the internal programming language in the FLAC code called FISH (FlacISH) (Itasca Consulting Group, Inc., 2019), this algorithm is written in the form of a FISH and implemented in the FLAC code.

According to the selected stress level, the values of f_{vp}, f_p, and f_d are calculated based on the relationships presented in section 1. In the algorithm shown in Figure 5, the relations of strain and stress for each step are given. As can be seen, the algorithm has four computational steps as follows:

1. Evaluation of elastic-visco-plastic stresses;
2. Plastic surface corrections and new stresses;
3. Update the α_{vp};
4. Obtain new wing crack length and update damage parameter (Ω).

3. Determining model parameters

In this section, the calibration of the proposed constitutive model with the experimental results obtained from laboratory tests performed on gypsum samples is presented. Samples of gypsum are taken from Damavand region in the northeast Tehran in Iran. Table 1 presents the results of the XRF test on this type of gypsum. Also, according to laboratory tests performed on gypsum samples, the average uniaxial compressive strength was 18.6 MPa and the Brazilian tensile strength was 3.97 MPa.

Table 1. XRF test result

Mineral Oxides	Weight (%)
Na_2o	0.03
CaO	32.2
MgO	0.01
Fe_2O_3	0.05
Al_2O_3	0.02
SrO	0.06
SO_3	46.06
Loss on Ignition	21.53
Cl	0.04

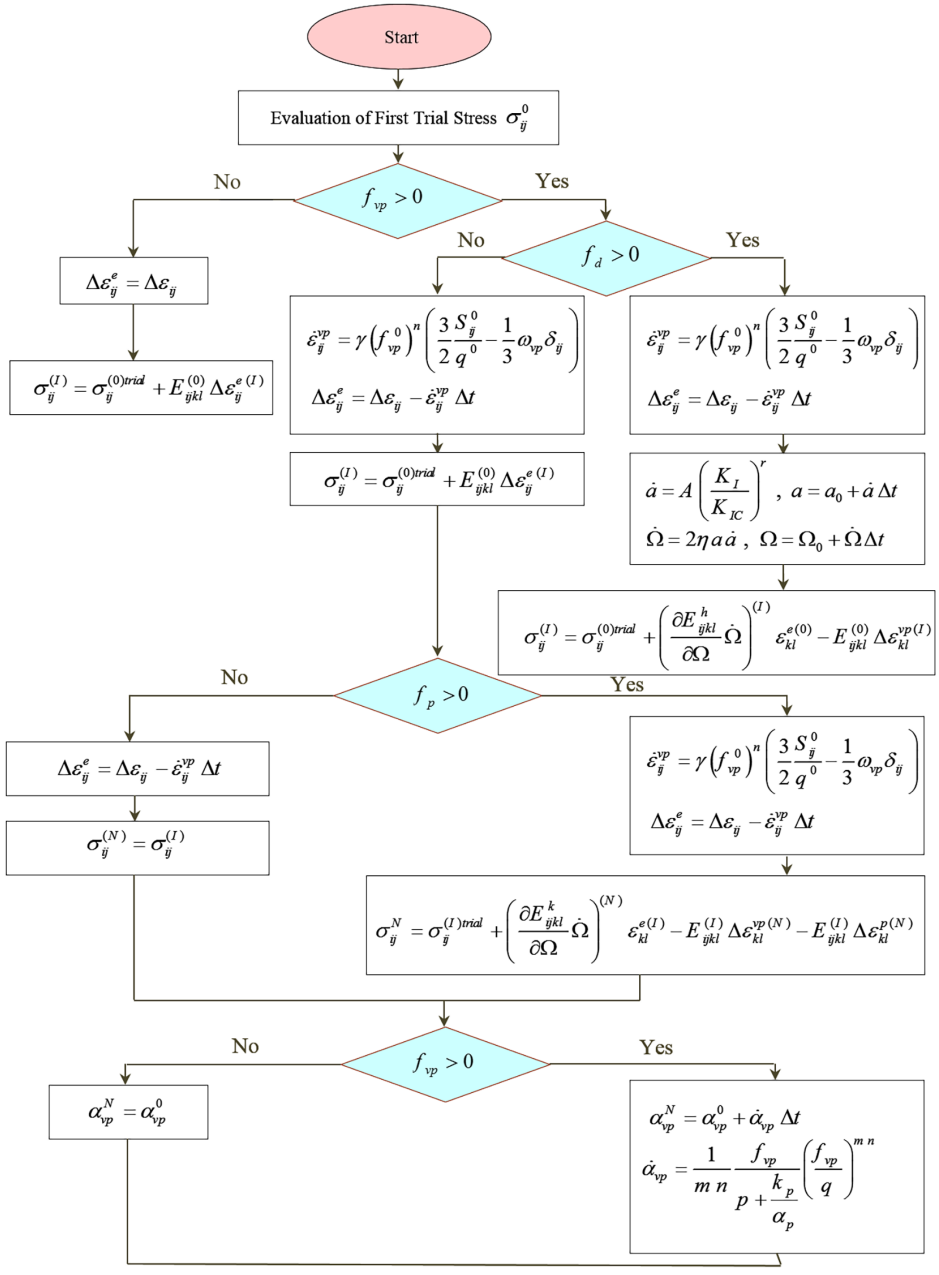

Figure 5. Computational algorithm of the mathematical model

The parameters of the proposed constitutive model are divided into four groups: (1) elastic parameters (E, υ); (2) plastic parameters $(\alpha_p, k_p, \sigma_t, \omega_p)$; (3) visco-plastic parameters $(\gamma, m, n, \ell, \omega_{vp})$; and (4) fracture toughness and sub-critical crack growth parameters $(K_{Ic}, A, r, \eta, 2s, \beta, \mu, \theta, a)$:

1) Elastic parameters (E, υ): the elastic modulus and Poisson's ratio of material are obtained using the results of uniaxial compression test performed on gypsum rock samples in accordance with the values presented in Table 2.
2) Plastic parameters $(\alpha_p, k_p, \sigma_t, \omega_p)$: (α_p, k_p) are obtained according to Eqn (6) and using Mohr-Coulomb failure criterion mechanical parameters (c, ϕ). Mohr-Coulomb criterion parameters are also obtained using triaxial tests performed on gypsum specimens. Tensile strength (σ_t) is also obtained using the result of the Brazilian tensile test. The plastic dilatancy parameter (ω_p) is considered zero due to the impossibility of measuring the ratio of the volumetric plastic strain increment to the deviatoric plastic strain increment.
3) Visco-plastic parameters $(\gamma, m, n, \ell, \omega_{vp})$: to obtain the visco-plastic dilatancy parameter (ω_{vp}), the lateral strain versus axial strain diagram is plotted in the creep test. This curve is then interpolated by a straight line. Using the slope of this line, the visco-plastic dilatancy parameter can be obtained. By drawing the axial strain rate against time, the shape factor (m) is obtained. Other visco-plastic parameters (γ, n, ℓ) are obtained by fitting the results of

Table 2. Parameters of the model

Parameter	Index	Unit	Value
Elastic modulus	E	MPa	33274
Poisson's ratio	υ	–	0.271
Slope of the Drucker-Pragers plastic yield surface in the q-p plane	α_p	–	0.788
q-intercept of the Drucker-Pragers plastic yield surface	k_p	MPa	18.628
Brazilian tensile strength	σ_t	MPa	3.97
Plastic dilatancy	ω_p	–	0
Fluidity parameter	γ	–	2.197e-8
Shape factor	m	–	1.002
Load factor	n	–	1.426
Time stretching factor	ℓ	–	79.295
Visco-plastic dilatancy	ω_{vp}	–	0.012
Fracture toughness (mode I)	K_{Ic}	MPa $\sqrt{\text{m}}$	0.612
Sub-critical crack growth parameter	A	m/s	0.5
Sub-critical crack growth index	r	–	25
Flaw density	η	m^{-2}	4.26E9
Flaw size	$2s$	μm	150.6
Flaw orientation	β	$(^0)$	45
coefficient of friction on the flaw surface	μ	–	0.2

the uniaxial creep test performed on gypsum and the results of numerical analysis by means of a numerical optimization procedure.

4) Fracture toughness and sub-critical crack growth parameters $(K_{Ic}, A, r, \eta, 2s, \beta, \mu, \theta)$: fracture toughness (K_{Ic}) of gypsum measured via the semi-circular bend (SCB) test. The sub-critical crack growth parameter (A) and sub-critical crack growth index (r) have been selected based on the suggestions made by Ko and Kemeny (2013) and Ko and Lee (2020). Flaw density (η) and Flaw length $(2s)$ values were obtained based on the analysis of images obtained by scanning electron microscope (SEM). Flaw orientation (β), coefficient of friction on the flaw surface (μ), and wing crack angle (θ) are selected based on the values presented in the literature (Paliwal & Ramesh, 2008; Ashby & Hallam, 1986; Horii & Nemat-Nasser, 1986). Table 2 lists the model parameters.

4. Validation and results

The proposed constitutive model with the sub-critical crack growth model, is used in a uniaxial creep test. According to the symmetry conditions of the specimen in this test, only a quarter of the specimen is modeled (Figure 6). Numerical modeling and analysis have been done by FLAC^{2D} code.

Because the uniaxial compressive strength of gypsum specimens is 18.6 MPa, the sample is loaded to an axial stress of 13 MPa, which is equivalent to 70% of the uniaxial compressive strength of the gypsum specimen. Then the stress states are kept constant and the strains are measured over time.

Figure 7 shows the evolution of the damage parameter versus the loading time. Figure 8 shows the increase in wing crack length over time. The increase in wing crack length occurs simultaneously with the growth of the damage parameter. Also, Figure 9 shows the changes in the ratio of $\frac{K_I}{K_{Ic}}$ versus time, as can be seen, this ratio decreases slightly during the loading period, which is accompanied by a steady and gradual increase in wing crack length. Figure 10 shows the creep curve obtained from laboratory data with the fitted curve of the theoretical-numerical model. As can be seen the adaptation is very good.

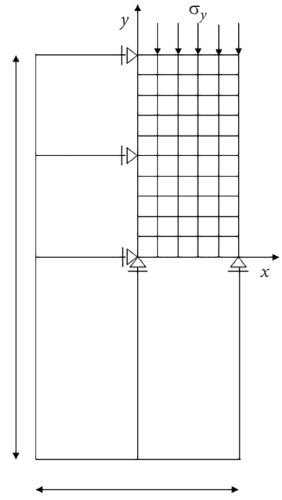

Figure 6. Loading and boundary conditions for a quarter of the model

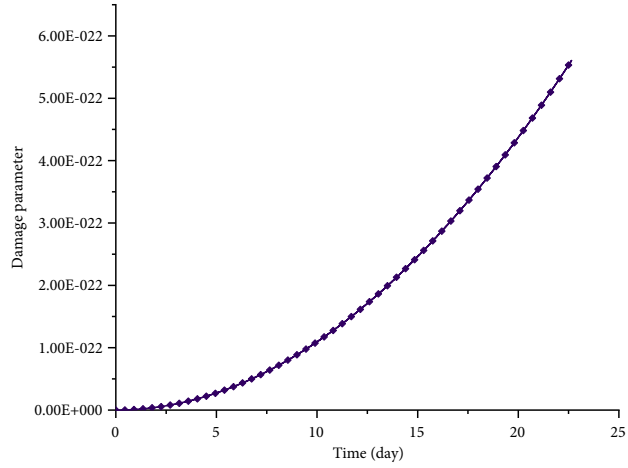

Figure 7. Evolution of damage parameter with time

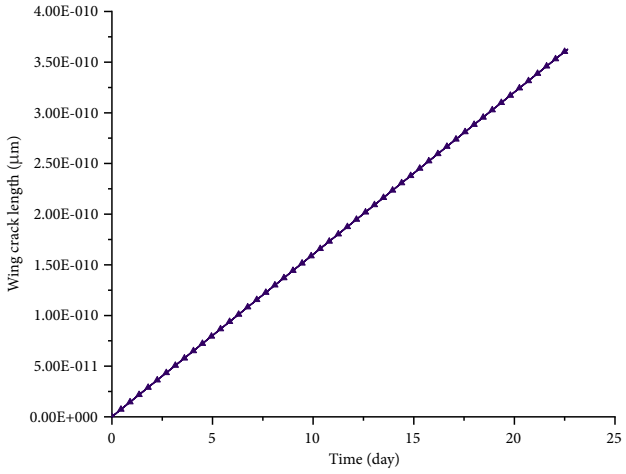

Figure 8. Evolution of wing crack length with time

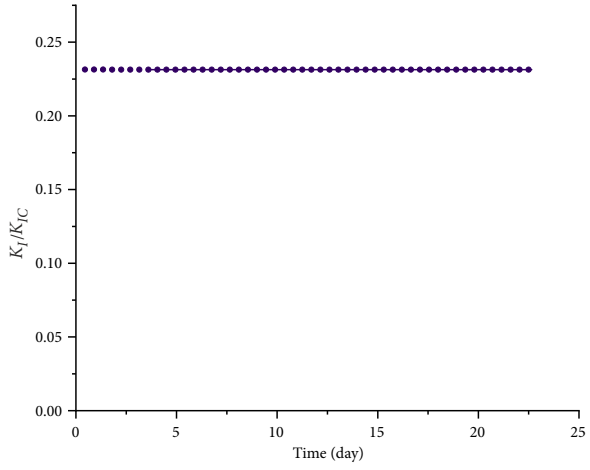

Figure 9. Evolution of normalized stress intensity factor versus time

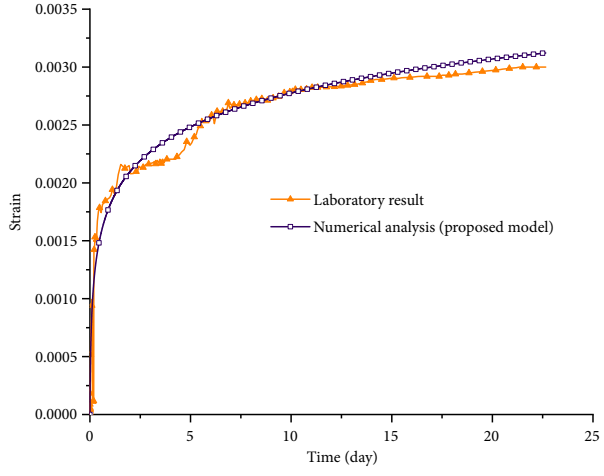

Figure 10. Creep curves, comparison between the results obtained from the laboratory data with the fitted curve of the proposed model

Conclusions

In this paper a mathematical model for predicting rock time-dependent behavior is presented. The proposed model is a combination of elastic-visco-plastic model based on Perzyna's over-stress theory (Perzyna, 1966) and stress hardening law. Damage during creep is investigated using a micro-mechanical damage model. In the micro-mechanical damage model, the growth of wing cracks occurs at the tips of flaws that are uniformly distributed in the material. The growth of wing cracks occurs before the stress intensity factor reaches its critical value. The growth of wing cracks during creep increases the strain and damage parameter. After determining the model parameters and calibration using experiments performed on gypsum samples, it was observed that the creep curve obtained from the laboratory results is in good agreement with the fitted creep curve of the theoretical-numerical model. According to the results, it was observed that the length of the wing crack and the failure parameter increase during the primary and secondary stages of creep, the rate of increase of wing crack length in both stages of creep test is constant but the rate of increase of damage parameter in the secondary stage of creep is higher than the primary stage.

References

Afrouz, A., & Harvey, J. M. (1974). Rheology of rocks within the soft to medium strength range. *International Journal of Rock Mechanics and Mining Sciences & Geomechanics Abstracts*, *11*, 281–290. https://doi.org/10.1016/0148-9062(74)90230-7

Ashby, M. F., & Hallam, S. D. (1986). The failure of brittle solids containing small cracks under compressive stress states. *Acta Metallurgica*, *34*(3), 497–510. https://doi.org/10.1016/0001-6160(86)90086-6

Aydan, Ö. (2016). *Time-dependency in rock mechanics and rock engineering* (1st ed.). CRC Press. https://doi.org/10.1201/9781315375151

Aydan, Ö., Ito, T., Özbay, U., Kwasniewski, M., Shariar, K., Okuno, T., Özgenoğlu, A., Malan, D. F., & Okada, T. (2014). ISRM suggested methods for determining the creep characteristics of rock. *Rock Mechanics and Rock Engineering*, *47*(1), 275–290. https://doi.org/10.1007/s00603-013-0520-6

Debernardi, D., & Barla, G. (2009). New viscoplastic model for design analysis of tunnels in squeezing conditions. *Rock Mechanics and Rock Engineering*, *42*(2), 259. https://doi.org/10.1007/s00603-009-0174-6

Feng, W.-l., Qiao, C., Niu, S., Yang, Z., & Wang, T. (2020). An improved nonlinear damage model of rocks considering initial damage and damage evolution. *International Journal of Damage Mechanics*, *29*, 1117–1137. https://doi.org/10.1177%2F1056789520909531

Gioda, G., & Cividini, A. (1996). Numerical methods for the analysis of tunnel performance in squeezing rocks. *Rock Mechanics and Rock Engineering*, *29*(4), 171–193. https://doi.org/10.1007/BF01042531

Goodman, R. E. (1989). *Introduction to rock mechanics* (2nd ed.). John Wiley & Sons Ltd.

Griggs, D. T., & Coles, N. E. (1954). *Creep of single crystals of ice* (SIPRE Report, 11). U.S. Army Snow, Ice, and Permafrost Research Establishment.

Gross, D., & Seelig, T. (2018). *Fracture mechanics: With an introduction to micromechanics* (3rd ed.). Springer. https://doi.org/10.1007/978-3-319-71090-7

Hasanzadehshooiili, H., Lakirouhani, A., & Medzvieckas, J. (2012). Evaluating elastic-plastic behaviour of rock materials using hoek–brown failure criterion. *Journal of Civil Engineering and Management*, *18*(3), 402–407. https://doi.org/10.3846/13923730.2012.693535

Horii, H., & Nemat-Nasser, S. (1986). Brittle failure in compression: splitting faulting and brittle-ductile transition. *Philosophical Transactions of the Royal Society of London. Series A, Mathematical and Physical Sciences*, *319*, 337–374. https://doi.org/10.1098/rsta.1986.0101

Hou, R., Zhang, K., Tao, J., Xue, X., & Chen, Y. (2019). A nonlinear creep damage coupled model for rock considering the effect of initial damage. *Rock Mechanics and Rock Engineering*, *52*(5), 1275–1285. https://doi.org/10.1007/s00603-018-1626-7

Huang, M., Zhan, J. W., Xu, C. S., & Jiang, S. (2020). New creep constitutive model for soft rocks and its application in the prediction of time-dependent deformation in tunnels. *International Journal of Geomechanics*, *20*(7), 04020096. https://doi.org/10.1061/(ASCE)GM.1943-5622.0001663

Itasca Consulting Group, Inc. (2019). *FLAC — Fast Lagrangian analysis of continua* (Ver. 8.1). Itasca.

Kemeny, J. (1991). A model for non-linear rock deformation under compression due to sub-critical crack growth. *International Journal of Rock Mechanics and Mining Sciences & Geomechanics Abstracts*, *28*, 459–467. https://doi.org/10.1016/0148-9062%2891%2991121-7

Ko, T. Y., Einstein, H., & Kemeny, J. (2006). Crack coalescence in brittle material under cyclic loading. In *Proceedings of the 41st U.S. Rock Mechanics Symposium* (Paper ARMA 06-930). Golden, CO.

Ko, T. Y., & Kemeny, J. (2013). Determination of the subcritical crack growth parameters in rocks using the constant stress-rate test. *International Journal of Rock Mechanics and Mining Sciences*, *59*, 166–178. https://doi.org/10.1016/j.ijrmms.2012.11.006

Ko, T. Y., & Lee, S. S. (2020). Characteristics of crack growth in rock-like materials under monotonic and cyclic loading conditions. *Applied Sciences*, *10*(2), 719. https://doi.org/10.3390/app10020719

Kranz, R. L. (1979). Crack growth and development during creep of Barre granite. *International Journal of Rock Mechanics and Mining Sciences & Geomechanics Abstracts*, *16*(1), 23–35. https://doi.org/10.1016/0148-9062(79)90772-1

Kranz, R. L. (1980). The effects of confining pressure and stress difference on static fatigue of granite. *Journal of Geophysical Research: Solid Earth*, *85*(B4), 1854–1866. https://doi.org/10.1029/JB085iB04p01854

Lakirouhani, A., & Hasanzadehshooiili, H. (2011). Review of rock strength criteria. In *Proceedings of the 22nd World Mining Congress & Expo* (pp. 473–482), Istanbul, Turkey.

Lemaitre, J., & Chaboche, J. (1990). *Mechanics of solid materials*. Cambridge University Press. https://doi.org/10.1017/CBO9781139167970

Lockner, D. (1993). Room temperature creep in saturated granite. *Journal of Geophysical Research: Solid Earth*, *98*(B1), 475–487. https://doi.org/10.1029/92JB01828

Lockner, D. A., & Madden, T. R. (1991). A multiple-crack model of brittle fracture: 2. Time-dependent simulations. *Journal of Geophysical Research: Solid Earth*, *96*(B12), 19643–19654. https://doi.org/10.1029/91JB01641

Lomnitz, C. (1956). Creep measurements in igneous rocks. *The Journal of Geology*, *64*(5), 473–479. https://doi.org/10.1086/626379

Ma, L., Wang, M., Zhang, N., Fan, P., & Li, J. (2017). A variable-parameter creep damage model incorporating the effects of loading frequency for rock salt and its application in a bedded storage cavern. *Rock Mechanics and Rock Engineering*, *50*, 2495. https://doi.org/10.1007/s00603-017-1236-9

Paliwal, B., & Ramesh, K. T. (2008). An interacting micro-crack damage model for failure of brittle materials under compression. *Journal of the Mechanics and Physics of Solids*, *56*(3), 896–923. https://doi.org/10.1016/j.jmps.2007.06.012

Olson, J. (1993). Joint pattern development: Effects of subcritical crack growth and mechanical crack interaction. *Journal of Geophysical Research*, *98*, 12251–12265. https://doi.org/10.1029/93JB00779

Pellet, F., Hajdu, A., Deleruyelle, F., & Besnus, F. (2005). A viscoplastic model including anisotropic damage for the time dependent behaviour of rock. *International Journal for Numerical and Analytical Methods in Geomechanics*, *29*(9), 941–970. https://doi.org/10.1002/nag.450

Perzyna, P. (1966). Fundamental problems in viscoplasticity. *Advances in Applied Mechanics*, *9*, 246–377. https://doi.org/10.1016/S0065-2156(08)70009-7

Robertson, E. C. (1955). Experimental study of the strength of rocks. *GSA Bulletin*, *66*(10), 1275–1314. https://doi.org/10.1130/0016-7606(1955)66[1275:ESOTSO]2.0.CO;2

Shao, J.-F., Chau, K. T., & Feng, X. T. (2006). Modeling of anisotropic damage and creep deformation in brittle rocks. *International Journal of Rock Mechanics and Mining Sciences*, *43*, 82–592. https://doi.org/10.1016/j.ijrmms.2005.10.004

Sterpi, D., & Gioda, G. (2009). Visco-plastic behaviour around advancing tunnels in squeezing rock. *Rock Mechanics and Rock Engineering*, *42*(2), 319–339. https://doi.org/10.1007/s00603-007-0137-8

Zhang, J.-Z., Zhou, X.-P., & Yin, P. (2019). Visco-plastic deformation analysis of rock tunnels based on fractional derivatives. *Tunnelling and Underground Space Technology*, *85*, 209–219. https://doi.org/10.1016/j.tust.2018.12.019